RSC Advances

PAPER

View Article Online
View Journal | View Issue

Cite this: *RSC Adv.*, 2026, **16**, 21478

Synthesis, and evaluation of novel low nanomolar isoindigo-based RET kinase inhibitors

Mazen Al Sulaibi,[a] Hamdi Nsairat,[a]* Jalal Zahra[b] and Mutasem O. Taha[c]*

Acquired resistance to selective kinase inhibitors remains a primary challenge in targeted cancer therapy. The clinical efficacy of potent rearranged during transfection (RET) inhibitors, for instance, is often attenuated by the emergence of on-target mutations, such as the V804L gatekeeper variant. To address this, a novel series of isoindigo-based compounds were designed, synthesized, and evaluated for RET kinase inhibitory activity. This effort led to the identification of compound **4c**, which demonstrated potent, low-nanomolar inhibition of wild-type RET kinase (IC_{50} = 13.7 nM) and retained, even enhanced, biochemical potency against the clinically relevant RET V804L gatekeeper mutant (IC_{50} = 5.2 nM). Kinase selectivity profiling confirmed that **4c** displays a favorable selectivity profile, with negligible activity against c-KIT, a common off-target associated with toxicity in less selective multi-kinase inhibitors. Molecular modelling provided a structural rationale for the enhanced potency against the V804L mutant. These findings identify compound **4c** as an early lead with promising biochemical potency in this initial exploration of isoindigo-based RET inhibitors. However, it should be noted that these results are based on biochemical (enzymatic) assays only, and further cell-based validation is required to assess the translational potential of this compound.

Received 9th February 2026
Accepted 4th April 2026

DOI: 10.1039/d6ra01152g

rsc.li/rsc-advances

1. Introduction

Kinases play a crucial role in regulating cell signaling, and their abnormal activation or overexpression is often linked to the development and progression of cancer.[1–3] The rearranged during transfection (RET) proto-oncogene encodes a receptor tyrosine kinase (RTK) that is a critical regulator of cell growth, differentiation, and survival.[4,5] Aberrant RET activation, driven by gene fusions or activating point mutations, is a validated oncogenic driver in a range of malignancies, most notably in 1–2% of non-small cell lung cancers (NSCLC) and the majority of medullary thyroid carcinomas (MTC).[6–8] The clinical validation of RET as a therapeutic target has culminated in the development and approval of highly selective inhibitors, such as selpercatinib and pralsetinib (Fig. 1), which have demonstrated impressive efficacy and have become the standard of care for patients with RET-altered cancers.[9,10] Despite this success, significant clinical challenges persist.[5] The emergence of acquired resistance, frequently mediated by secondary on-target mutations in the kinase domain, limits the duration of response.[5,6] Gatekeeper mutations at Val804 position (V804L/V804M) sterically hinder drug binding, while solvent-front mutations (*e.g.*, G810R/S/C) can also confer resistance to first-generation selective inhibitors.[6,10–14]

Recent efforts have focused on developing inhibitors capable of overcoming RET resistance mechanisms (Fig. 1). For example, alectinib effectively targets the gatekeeper mutations V804L and V804M, with IC_{50} values of 32 nM and 53 nM, respectively.[15] More advanced scaffolds, such as *N*-trisubstituted pyrimidines[16] and next-generation alkynyl nicotinamides,[12] have also shown potent low-nanomolar activity against both wild-type and mutant RET. The dual RET/VEGFR2 inhibitor Pz-1 exhibits sub-nanomolar potency;[17] however, its concurrent activity against VEGFR2 raises concerns regarding potential vascular toxicities.[5] In addition, the central nervous system (CNS) is a frequent site of metastasis, yet the efficacy of many RET inhibitors is limited by poor penetration across the blood–brain barrier, underscoring the urgent need for new agents with enhanced pharmacological and CNS-penetrant properties.[18]

The isoindigo core is recognized as a privileged scaffold in medicinal chemistry, with derivatives known to exhibit potent anticancer activity through the inhibition of various protein kinases.[19–22] In our previous work, we reported the first examples of isoindigo derivatives possessing RET kinase inhibitory activity, establishing a foundation for further optimization.[23] Building on these findings, the present study was undertaken to design and synthesize a new series of substituted isoindigo compounds as an initial exploration of the isoindigo scaffold against RET kinase. Our objective was to enhance potency against wild-type RET and, critically, to retain and even enhance biochemical potency

[a]*Pharmacological and Diagnostic Research Center, Faculty of Pharmacy, Al-Ahliyya Amman University, Amman 19328, Jordan. E-mail: h.alnseirat@ammanu.edu.jo*
[b]*Department of Chemistry, Faculty of Science, The University of Jordan, Amman, Jordan*
[c]*Department of Pharmaceutical Sciences, Faculty of Pharmacy, The University of Jordan, Amman 11942, Jordan. E-mail: mutasem@ju.edu.jo*

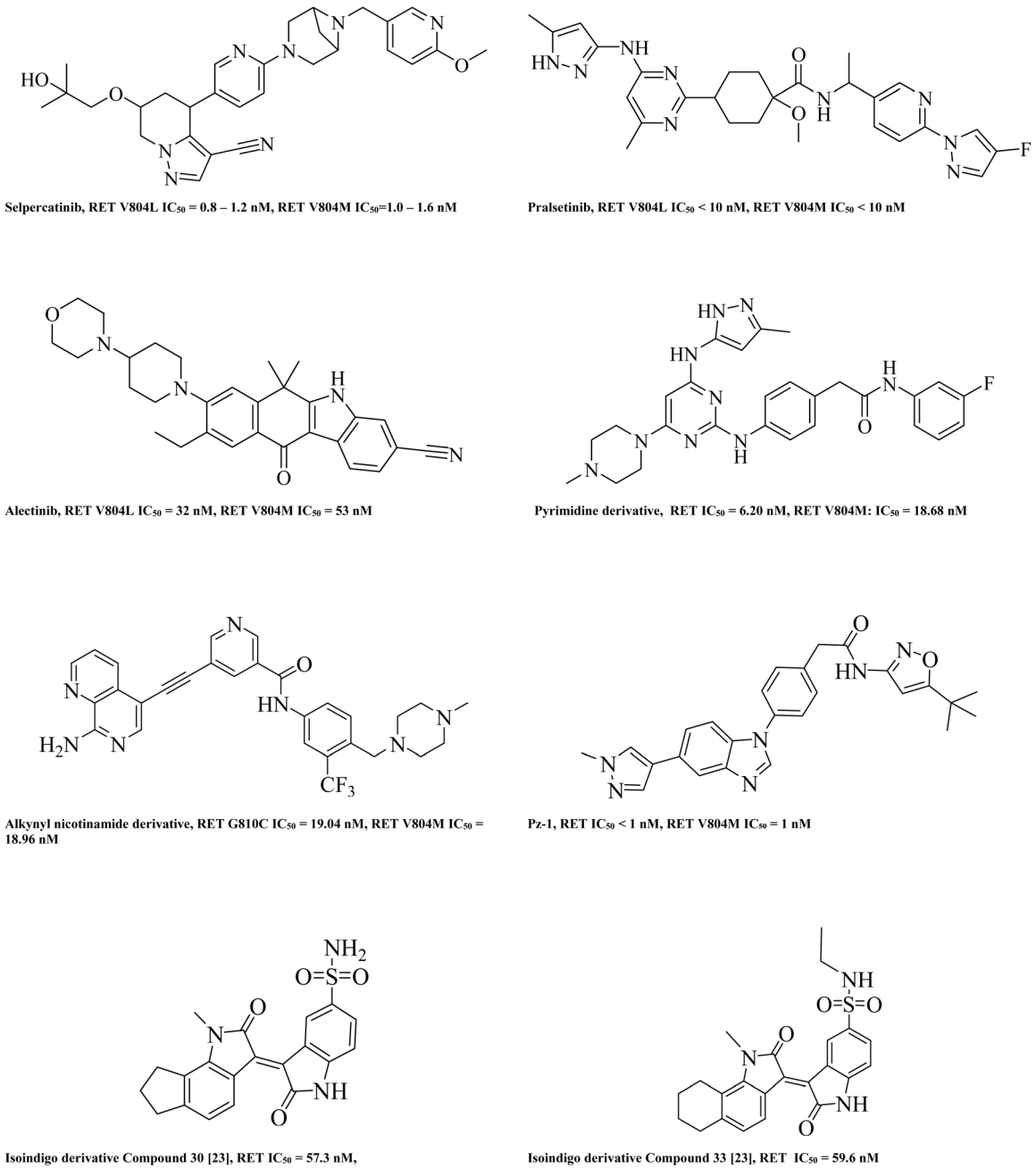

Fig. 1 Chemical structures of some RET inhibitors.

against the V804L gatekeeper mutant. In parallel, we aimed to comprehensively evaluate the kinase selectivity profile of these novel compounds to ensure their suitability as selective RET inhibitors. This work has led to the identification of an early lead compound with potent biochemical inhibitory activity against RET and its V804L mutant.

2. Results and discussion

2.1 Chemistry

The target isoindigo derivatives **4a–f** was synthesized *via* a straightforward and efficient acid-catalyzed aldol condensation of various substituted isatins **3a–d** with substituted oxindoles **2a–d** (Scheme 1). The required isatins were commercially available, while the sulfonamide-substituted oxindoles **2a–d** was prepared from oxindole in two steps (Scheme 1). Chlorosulfonation of oxindole afforded 2-oxoindoline-5-sulfonyl chloride **1** in 91% yield. Subsequent reaction of intermediate **1** with appropriate amines yielded the desired oxindoles **2a–d**. The structures of known oxindoles **2a–c** were confirmed by comparison of their NMR and mass spectral data with literature values.[24–26] The novel oxindole **2d** was fully characterized by ^{1}H NMR, ^{13}C NMR (see SI, Fig. S4).

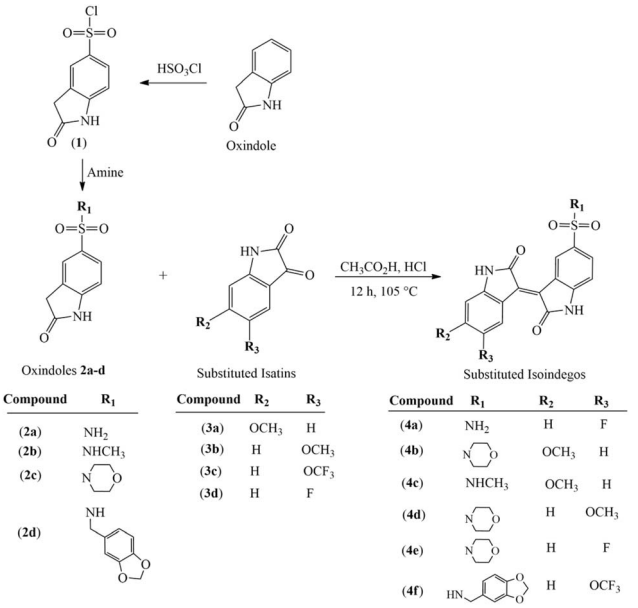

Scheme 1 Synthesis of substituted isoindigo derivatives **4a–f**.

The final isoindigo derivatives **4a–f** was obtained in yields ranging from 36% to 77% following condensation and purification. The formation of the target compounds was confirmed by comprehensive spectral analysis, including ^{1}H NMR, ^{13}C NMR, and DEPT experiments. The mass spectral data for all final compounds were in full accordance with their assigned structures (see Experimental section and SI, Fig. S5 to S10).

2.2 Biological evaluation and structure–activity relationship (SAR)

The newly synthesized compounds **4a–f** were first evaluated for their inhibitory activity against a panel of structurally related tyrosine kinases, including ABL1, VEGFR2, TRKC, FLT3, FLT3 D835Y, c-KIT, and RET (Table 1). The data revealed that the compounds exhibited varied inhibitory profiles. Notably, all synthesized compounds showed negligible inhibition of c-KIT, which is a highly desirable feature, as c-KIT inhibition is associated with potentially severe side effects such as cardiotoxicity and myelosuppression.[27–33]

Compounds **4a**, **4b**, and **4c** displayed the most promising activity, with significant inhibition of RET, TRKC, and the mutant FLT3 D835Y. The development of multi-kinase inhibitors targeting oncogenic pathways simultaneously can offer synergistic therapeutic effects and a strategy to address mechanisms of drug resistance at the biochemical level. However, the preliminary data clearly indicated that RET kinase was the most sensitive target for this series. The potent inhibition of TRKC (91% by **4c**) and the resistance-conferring FLT3 D835Y mutant (80% by **4c**) are also noteworthy secondary findings. While a full characterization of these activities with IC50 determination is beyond the scope of this initial RET-focused study, the data suggest a potential for this scaffold in a multi-targeted therapeutic strategy. A detailed investigation into this polypharmacology is a key objective for future research.

Given the potent activity against wild-type RET, we next evaluated all compounds against clinically relevant RET mutants: V804L, V804M, and M918T (Table 1). The most active compounds from the initial screen, **4a**, **4b**, and **4c**, demonstrated remarkable inhibitory activity against the V804L gatekeeper mutant, with compound **4c** achieving 100% inhibition at 10 μM. In contrast, activity against the V804M and M918T mutants was moderate. The less active compounds (**4d–f**) were not pursued further against the mutant panel.

To quantify their potency, the IC_{50} values for compounds **4a**, **4b**, and **4c** were determined against both wild-type RET and the RET V804L mutant (Table 1). The corresponding dose–response curves for these determinations are provided in the SI (Fig. S1). The results highlighted a clear structure–activity relationship. Compound **4a**, with an unsubstituted sulfonamide, was the least potent of the three (IC_{50} = 889.0 nM *vs.* WT RET). Replacing this with a morpholine group in **4b** improved potency significantly (IC_{50} = 258.2 nM). The most potent compound was **4c**, which features a simple *N*-methylsulfonamide group, exhibiting an IC_{50} of 13.7 nM against wild-type RET.

Intriguingly, the potency of all three compounds increased against the V804L mutant. This effect was most pronounced for **4c**, which inhibited RET V804L with an outstanding IC_{50} of 5.2 nM, making it a highly potent dual inhibitor of both wild-

Table 1 Bioactivities of prepared compounds against cancer related tyrosine kinases

	% inhibition at 10 μM[a]										IC$_{50}$ values[a,b] (nM)	
Compound	ABL1	KDR (VEGFR2)	NTRK3 (TRKC)	FLT3	FLT3 D835Y	c-KIT	RET	RET V804L	RET V804M	RET M918T	RET	RET V804L
4a	65	17	55	27	36	8	**75**	**86**	47	33	889.0	389.2
4b	14	12	83	37	83	4	**82**	**94**	34	27	258.2	53.6
4c	37	17	91	43	80	3	**97**	**100**	55	55	13.7	5.2
4d	33	25	26	13	27	2	29	ND[a]	ND	ND	ND	ND
4e	14	20	34	20	31	−1	42	ND	ND	ND	ND	ND
4f	41	6	27	9	21	10	34	ND	ND	ND	ND	ND

[a] Each value represents the average of two independent measurements (n = 2). IC_{50} values were determined by nonlinear regression of dose–response curves (Fig. S1). ND: not determined. [b] Staurosporine was used as standard (control) inhibitor with corresponding IC_{50} values of 2.89 nM and 1.99 nM against RET and RET V804L, respectively.

type and a key resistance mutant. The ability to potently inhibit the V804L gatekeeper mutant, which blocks drug access in many inhibitors,[9] is an encouraging feature for the further development of this scaffold as a RET-targeted inhibitor.

2.3 Docking-guided exploration and structure–activity relationship

To rationalize the observed biological activities and understand the structural basis of inhibition, molecular docking studies were performed for all synthesized compounds (**4a–f**) against both wild-type RET and the V804L mutant. First, the validity of our docking protocol was confirmed by re-docking the co-crystallized ligand selpercatinib into the active site of the wild-type RET kinase crystal structure (PDB: 7JU6). The docked pose showed excellent alignment with the crystallographic pose, demonstrating the reliability of the protocol (SI Fig. S2-A, RMSD = 1.34 Å). As no crystal structure exists for the V804L mutant, a homology model was generated by performing an *in silico* mutation of Val804 to Leu804 on the 7JU6 structure. The docking protocol was similarly validated on this model (SI Fig. S2-A, RMSD = 1.072 Å), ensuring its suitability for further studies.

The binding site was defined as a selpercatinib-centered sphere in the RET ATP pocket, and each ligand was sampled in 10 initial conformations using the CHARMm-based CDOCKER protocol, followed by high-temperature molecular-dynamics sampling, simulated annealing, and final energy minimization. For the V804L model, replacement of Val804 by Leu was followed by local minimization of residues surrounding the mutation site to relieve unfavorable contacts before comparative docking.

Docking into wild-type RET kinase. The predicted binding modes of the most active compounds (**4a**, **4b**, and **4c**) within the ATP-binding site of wild-type RET are illustrated in SI Fig. S2-B, S2-C and 2, respectively. All three ligands adopted a broadly similar orientation, anchored by a key hydrogen bond—either with the carboxylate of the DFG motif residue Asp892, as in **4a** and **4c** (SI Fig. S2-B and 2, respectively), or with the ammonium group of the nearby Lys758, as in **4b** and **4c** (SI Fig. S2-C and 2, respectively). Compounds **4a** and **4b** each formed three additional hydrogen bonds with the backbone carbonyls and amide NH groups of Glu805, Leu730, and Ala807. In contrast, **4c** appeared to compensate for the absence of these three interactions through hydrogen bonding and π–π stacking with the phenolic side chain of Tyr806. The fluoro substituent in **4a** uniquely engaged in hydrogen bonding with the backbone NH of Gly733. In all cases, the docked poses revealed hydrophobic contacts with the side chains of Leu881, Val738, and Leu730, while the sulfonamide tail extended toward the solvent-exposed region.

The docking poses of the inactive analogues **4d–f** (SI Fig. S3) indicate markedly less favorable binding. Bulky peripheral substituents on these compounds introduce steric clashes within the ATP pocket and displace the isoindigo core into suboptimal orientations, disrupting key hydrogen-bonding interactions to Glu805, Leu730, Ala807, Tyr806 and Gly733 seen with potent analogues. These structural perturbations reduce predicted interaction energies and coherently explain the compounds' poor inhibitory activity.

Docking into the RET V804L mutant kinase. Importantly, the modeled structural consequence of the V804L substitution is a localized increase in steric bulk and hydrophobic character at the gatekeeper region rather than a global reorganization of the ATP-binding site. The docking model therefore suggests that **4c** accommodates the mutation through local shape complementarity: the curved isoindigo scaffold presents its concave face toward Leu804, thereby minimizing steric clash while preserving the Asp892/Lys758/Tyr806 interaction network that stabilizes binding.

To understand the high potency of our lead compounds against the V804L gatekeeper mutant, compounds **4a**, **4b**, and **4c** were docked into the V804L homology model (SI Fig. S2-D, S2-E and 3, respectively). The mutation from valine to the slightly larger leucine at the gatekeeper position can sterically block many inhibitors. However, the isoindigo scaffold appears well-suited to accommodate this change.

The docked pose of the most potent compound, **4c**, in the V804L mutant (Fig. 3) reveals that it retains the critical hydrogen bonds with Asp892 of the DFG motif, the ammonium group of Lys758, and the phenolic side chain of Tyr806. Notably, the crescent-shaped isoindigo backbone orients its concave face toward Leu804, allowing the scaffold to accommodate the bulkier gatekeeper residue without steric hindrance. This preserved binding mode accounts for its outstanding potency against the mutant (IC_{50} = 5.2 nM). A comparable adaptation was observed for compounds **4a** and **4b** (SI Fig. S2-D and S2-E), consistent with their enhanced IC_{50} values against V804L relative to wild-type RET.

The calculated CDOCKER interaction energies (SI Table S1) provide qualitative support for these observations. It should be noted that CDOCKER interaction energies are inherently semi-quantitative; therefore, we emphasize the consistent qualitative trends rather than the absolute magnitudes of the energy differences. The interaction energies for compounds **4b** and **4c** are more favourable in the mutated RET V804L model compared to the wild-type, which aligns with the experimental data showing enhanced potency against the mutant kinase. This qualitative trend is consistent with the possibility that the subtle conformational changes induced by the V804L mutation may create a more complementary binding surface for this specific chemical scaffold.

3. Experimental section

3.1 General

All reagents and solvents were obtained from commercial sources and used without further purification. NMR spectra (^1H, ^{13}C, DEPT) were recorded on a Bruker Avance-III 500 MHz spectrometer. Chemical shifts (δ) are reported in ppm relative to TMS as an internal standard; coupling constants (J) are in Hertz. High-resolution mass spectra (HRMS) were measured using the electrospray ion trap (ESI) technique by collision-induced dissociation on a Bruker APEX-IV (7 tesla) instrument. All

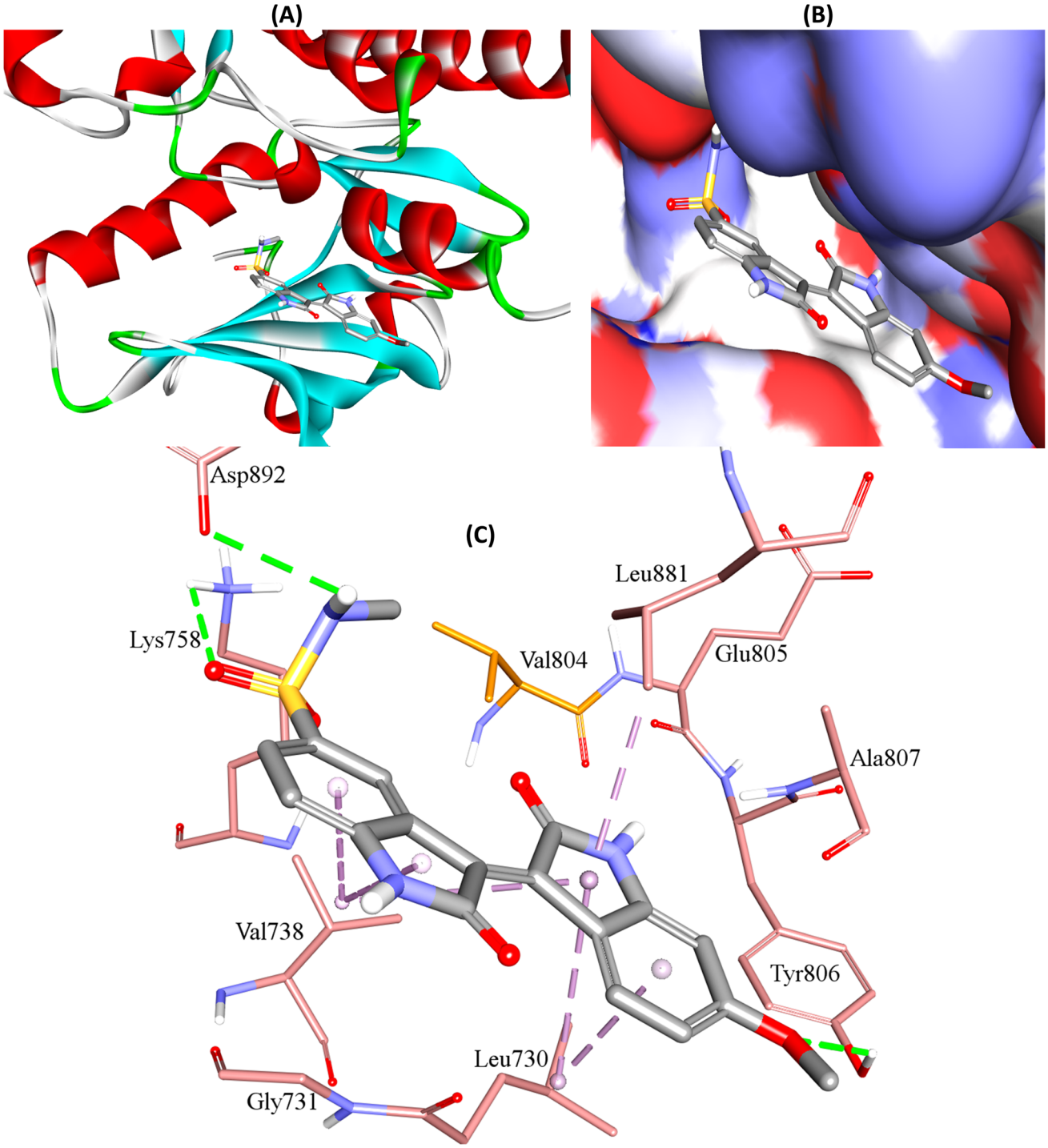

Fig. 2 Docked pose of **4c** into wild type RET kinase. (A) Panoramic view of the docked complex. (B) The docked ligand within the binding pocket covered by Connolly surface solvent accessible surface. (C) Detailed view of the docked complex showing interaction details. Hydrogen bonds are represented as green dotted lines; hydrophobic interactions are represented as pink dotted lines.

final compounds were of >95% purity as determined by HPLC analysis.

3.2 Synthesis

Synthesis of sulfonamide substituted oxindoles

*Synthesis of 2-oxoindoline-5-sulfonyl chloride (**1**).* In a controlled manner, oxindole (6.7 g, 50 mmol) was gradually introduced into chlorosulfonic acid (13.3 mL) while ensuring that the reaction temperature remained below 30 °C. Following the addition, the reaction mixture was stirred at ambient temperature for 1.5 h, then heated to 68 °C and stirred for an additional hour. Subsequently, the mixture was cooled to 0 °C, and approximately 30 g of ice was incrementally incorporated with continuous stirring. The resulting precipitate was isolated

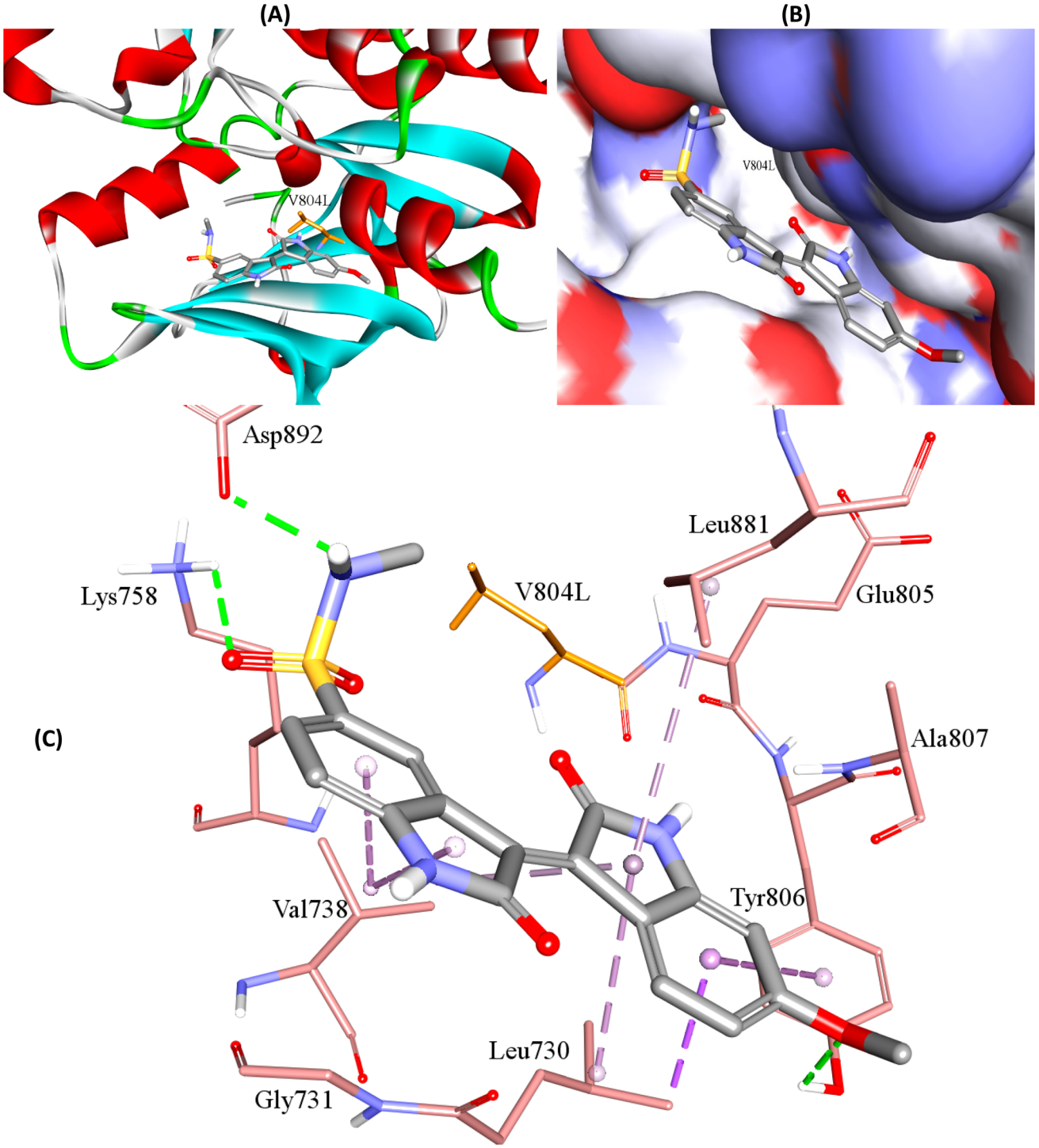

Fig. 3 Docked pose of **4c** into V804L RET kinase. (A) Panoramic view of the docked complex. (B) The docked ligand within the binding pocket covered by Connolly surface solvent accessible surface. (C) Detailed view of the docked complex showing interaction details. Hydrogen bonds are represented as green dotted lines; hydrophobic interactions are represented as pink dotted lines. The V804L mutation site is shown in gold yellow.

via filtration and washed with water, affording compound **1** in a yield of 91%. Compound **1** was utilized in subsequent reactions without further purification. Analytical data including NMR and MS spectra are consistent with literature values.[24]

Preparation of compounds 2a–d. A solution of 2-oxoindoline-5-sulfonyl chloride **1** (5 mmol) in 5 mL of ethanol was prepared and stirred. Subsequently, a solution of the corresponding amine (15 mmol) in 5 mL of ethanol was added to the reaction mixture. Notably, methylamine was provided as

40% aqueous solutions, and ammonium hydroxide as a 25% aqueous solution, while other amines were used in pure form. The resulting suspension was stirred at room temperature for 12 h. Following this, the mixture was concentrated, and the resulting solid was collected by suction filtration. The residual material underwent purification *via* crystallization from a solvent mixture of acetone and water (2 : 1), ultimately yielding the desired compounds (**2a–d**).

2-Oxoindoline-5-sulfonamide (2a). 2-Oxoindoline-5-sulfonamide (**2a**) was prepared using compound **1** and ammonium hydroxide 25% in water as starting materials. Yield 74%, the physiochemical data (NMRs, MS data) consistent with the literature.[25,26,34]

***N*-Methyl-2-oxoindoline-5-sulfonamide (2b).** *N*-Methyl-2-oxoindoline-5-sulfonamide (**2b**) was prepared using compound **1** and methylamine as starting materials. Yield 88%, the physiochemical data (NMRs, MS data) consistent with the literature.[24–26]

5-(Morpholinosulfonyl)indolin-2-one (2c). 5-(Morpholinosulfonyl)indolin-2-one (**2c**) was prepared using compound **1** and morpholine as starting materials. Yield 81%, the physiochemical data (NMRs, MS data) for Medicinal Chemistry Research this compound were consistent with those reported in the literature.[25]

***N*-(Benzo[*d*][1,3]dioxol-5-ylmethyl)-2-oxoindoline-5-sulfonamide (2d).** *N*-(Benzo[*d*][1,3]dioxol-5-ylmethyl)-2-oxoindoline-5-sulfonamide (**2d**) was prepared using compound **1** and benzo[*d*][1,3]dioxol-5-ylmethanamine, yield 70%, ^{1}H NMR (DMSO-d_6): δ = 3.81 (s, 4H), 4.06 (s, 2H), 6.13 (s, 2H), 6.89 (d, J = 7.6 Hz, 1H), 6.93 (s, 1H), 6.98 (d, J = 7.7 Hz, 1H), 7.30 (d, J = 7.9 Hz, 1H), 8.13 (br s, 1H). ^{13}C NMR (DMSO-d_6, 125 MHz): δ = 26.57, 35.40, 46.45, 101.33, 108.29, 108.52, 108.57, 121.47, 122.90, 127.66, 131.88, 134.27, 146.69, 147.55, 148.53, 175.02.

3.3 Synthesis of substituted isoindigos 4a–f

Substituted isatins (**3a–d**) (0.70 mmol) and substituted sulfonamide oxindoles (**2a–d**) (0.70 mmol) were suspended in 10 mL of glacial acetic acid, to which a catalytic amount of concentrated hydrochloric acid was added. The resulting mixture was stirred at 105 °C for 12 h, then cooled and diluted with 30 mL of water. The ensuing precipitate was isolated by filtration, washed successively with methanol: water (1 : 1) (20 mL) and dichloromethane : hexane (2 : 1) (20 mL), and subsequently dried to obtain the desired isoindigo derivatives **4a–f**. Purification of the obtained compounds was achieved through column chromatography, utilizing a gradient elution system composed of hexane, dichloromethane, ethyl acetate, and acetonitrile. SI Fig. S5–S10 depict the corresponding NMR and mass spectral data for validation.

(*E*)-5′-Fluoro-2,2′-dioxo-[3,3′-biindolinylidene]-5-sulfonamide (4a). (*E*)-5′-Fluoro-2,2′-dioxo-[3,3′-biindolinylidene]-5-sulfonamide (**4a**) prepared by the condensation of compound **2a** and compound **3d**. ^{1}H NMR (DMSO-d_6, 500 MHz) δ = 6.80 (s, 1H), 6.95 (ps t 1H), 6.91 (t, J = 8.93 Hz, 1H), 7.20 (s, 2H), 7.79 (ps t, 1H), 8.90 (d, J = 10.3 Hz, 1H), 9.62 (d, J = 10.5 Hz, 1H), 10.90 (s, 1H), 11.30 (s, 1H). ^{13}C NMR (DMSO-d_6, 125 MHz): δ = 110.16, 110.7 (d, $^3J_{C-F}$ = 8.0 Hz), 116.6 (d, $^2J_{C-F}$ = 28.3 Hz), 120.0 (d, $^2J_{C-F}$ = 24.1 Hz), 121.4, 122.5 (d, $^3J_{C-F}$ = 8.0 Hz), 127.9, 131.4, 133.5, 134.7, 141.5, 147.2, 157.04 (d, $^1J_{C-F}$ = 233.0 Hz), 169.2, 169.6. HRMS (ESI) *m*/*z*: calculated for $C_{16}H_{10}FN_3O_4S$, $[M + Na]^+$: 382.02683, found 382.02807.

(*E*)-6′-Methoxy-5-(morpholinosulfonyl)-[3,3′-biindolinylidene]-2,2′-dione (4b). (*E*)-6′-Methoxy-5-(morpholinosulfonyl)-[3,3′-biindolinylidene]-2,2′-dione (**4b**) prepared by the condensation of compound **2c** and compound **3a**. ^{1}H NMR (DMSO-d_6, 500 MHz) δ = 3.00 (s, 4H), 3.46 (s, 3H), 3.74 (s, 4H), 6.50 (s, 1H), 6.65 (d, J = 7.86 Hz, 1H), 7.15 (d, J = 8.10 Hz, 1H), 7.77 (d, J = 7.90 Hz, 1H), 9.16 (d, J = 7.90 Hz, 1H), 9.56 (s, 1H), 11.00 (s, 1H), 11.43 (s, 1H). ^{13}C NMR (DMSO-d_6, 125 MHz): δ = 64.4, 56.1, 65.8, 96.3, 107.7, 110.0, 115.1, 122.4, 127.0, 127.8, 131.5, 132.5, 135.6, 147.8, 164.4, 169.4, 170.2. HRMS (ESI) *m*/*z*: calculated for $C_{21}H_{19}N_3O_6S$, $[M + H]^+$: 442.10673, found 442.10349.

(*E*)-6′-Methoxy-*N*-methyl-2,2′-dioxo-[3,3′-biindolinylidene]-5-sulfonamide (4c). (*E*)-6′-Methoxy-*N*-methyl-2,2′-dioxo-[3,3′-biindolinylidene]-5-sulfonamide (**4c**) prepared by the condensation of compound **2b** and compound **3a**. ^{1}H NMR (DMSO-d_6, 500 MHz) δ = 2.55 (d, J = 4.47 Hz, 3H), 3.44 (s, 3H), 6.50 (s, 1H), 6.65 (d, J = 8.20 Hz, 1H), 7.11 (d, J = 8.10 Hz, 1H), 7.36 (d, J = 4.60 Hz, 1H), 7.81 (d, J = 7.85 Hz, 1H), 9.16 (d, J = 8.90 Hz, 1H), 9.63 (s, 1H), 11.00 (s, 1H), 11.35 (s, 1H). ^{13}C NMR (DMSO-d_6, 125 MHz): δ = 29.2, 56.1, 96.2, 107.6, 110.0, 115.2, 122.1, 127.1, 128.3, 130.5, 132.3, 132.4, 135.2, 146.6, 147.7, 164.3, 169.8, 170.1. HRMS (ESI) *m*/*z*: calculated for $C_{18}H_{15}N_3O_5S$, $[M + H]^+$: 386.08052, found 386.08533.

(*E*)-5-Methoxy-5′-(morpholinosulfonyl)-[3,3′-biindolinylidene]-2,2′-dione (4d). (*E*)-5-Methoxy-5′-(morpholinosulfonyl)-[3,3-biindolinylidene]-2,2′-dione (**4d**) prepared by the condensation of compound **2c** and compound **3b**. ^{1}H NMR (DMSO-d_6, 500 MHz) δ = 2.60 (s, 4H), 3.01 (ps t, 4H), 3.74 (t, J = 4.43 Hz, 4H), 6.86 (d, J = 8.45 Hz, 1H), 7.08, 7.10 (dd, J = 8.45 Hz, 1H), 7.16 (d, J = 8.25 Hz, 1H), 7.80, 7.82 (dd, J = 3.28 Hz, 1H), 8.92 (d, J = 2.45 Hz, 1H), 9.65 (s, 1H), 10.83 (s, 1H), 11.49 (s, 1H). ^{13}C NMR (DMSO-d_6, 125 MHz): δ = 46.4, 56.0, 65.8, 110.3, 110.5, 116.1, 119.8, 122.1, 122.5, 127.2, 129.3, 131.9, 132.5, 136.5, 139.1, 148.0, 154.5, 169.4, 169.5. HRMS (ESI) *m*/*z*: calculated for $C_{21}H_{19}N_3O_6S$, $[M + Na]^+$: 464.08868, found 464.08723.

(*E*)-5-Fluoro-5′-(morpholinosulfonyl)-[3,3′-biindolinylidene]-2,2′-dione (4e). (*E*)-5-Fluoro-5′-(morpholinosulfonyl)-[3,3′-biindolinylidene]-2,2′-dione (**4e**) prepared by the condensation of compound **2c** and compound **3d**. ^{1}H NMR (DMSO-d_6, 500 MHz) δ = 2.60 (s, 4H), 3.01 (ps t, 4H), 3.74 (t, J = 4.43 Hz, 4H), 6.94 (s, 1H), 6.96 (t, J = 4.3 Hz, 1H), 7.18 (d, J_{H-F} = 8.3 Hz, 1H), 7.35 (dd, J_{H-F} = 2.6 Hz, J_{H-H} = 8.3 Hz, 1H), 7.84 (dd, J_{H-H} = 8.3 Hz, J_{H-F} = 4.0 Hz, 1H), 9.0 (dd, J_{H-F} = 2.4 Hz, J_{H-H} = 7.9 Hz, 1H), 9.66 (s, 1H), 11.1 (s, 1H), 11.6 (s, 1H). ^{13}C NMR (DMSO-d_6, 125 MHz): δ = 46.4, 65.8, 110.4, 110.8, 116.7, 120.3, 122.1, 122.5, 127.4, 129.6, 132.9, 133.0, 135.3, 148.4, 158.4, 169.3, 169.5. HRMS (ESI) *m*/*z*: calculated for $C_{20}H_{16}FN_3O_5S$, $[M + Na]^+$: 452.06869, found 452.06887.

(*E*)-*N*-(Benzo[*d*][1,3]dioxol-5-ylmethyl)-2,2′-dioxo-5′-(trifluoromethoxy)-[3,3′ biindolinylidene]-5-sulfonamide (4f). (*E*)-

N-(Benzo[*d*][1,3]dioxol-5-ylmethyl)-2,2′-dioxo-5′-(trifluoromethoxy)-[3,3′ biindolinylidene]-5-sulfonamide (**4f**) prepared by the condensation of compound **2d** and compound **3c**. ^{1}H NMR (DMSO-d_6, 500 MHz) $\delta = 3.88$ (d, $J = 6.20$ Hz, 2H), 5.82 (s, 2H), 6.61 (d, $J = 7.85$ Hz, 1H), 6.66 (d, $J = 7.75$ Hz, 1H), 6.91 (t, $J = 8.93$ Hz, 1H), 7.36 (d, $J = 6.95$ Hz, 1H), 7.69, 7.71 (d, d $J = 3.23$ Hz, 1H), 7.95 (t, $J = 6.28$ Hz, 1H), 9.13 (s, 1H), 9.51 (s, 1H), 11.09 (s, 1H), 11.30 (s, 1H). ^{13}C NMR (DMSO-d_6, 125 MHz): $\delta = 46.49$, 101.2, 108.2, 108.6, 110.3, 110.9, 121.4, 121.5, 121.8, 122.6, 123.0, 126.6, 128.9, 131.8, 132.0, 133.8, 134.2, 134.3, 142.9, 144.0, 146.6, 147.5, 147.6, 169.2, 169.6.6. HRMS (ESI) *m*/*z*: calculated for $C_{25}H_{16}F_3N_3O_7S$, $[M + H]^+$: 560.07338, found 560.06955.

3.4 Biological evaluation procedures

***In vitro* enzyme assays.** The inhibitory activities of the synthesized compounds were evaluated against ABL1, KDR (VEGFR2), NTRK3 (TRKC), FLT3, FLT3-D835Y, RET, RET V804L, RET V804M, and RET M918T using the Invitrogen Z′-LYTE® Kinase Assay Kit, following the manufacturer's protocol.[35] Assays were performed at optimal kinase (2.7–4.7 nM) and ATP concentrations. Stock solutions of test compounds were prepared at 10 mM in DMSO and serially diluted to yield final concentrations ranging from 0.01 μM to 100 μM. The final DMSO concentration did not exceed 1% in the kinase reaction. IC_{50} values were calculated using nonlinear regression of log(-concentration) *vs.* inhibition percentage curves using GraphPad Prism 7.04. Staurosporine was used as a positive control.

3.5 Molecular docking study

Molecular docking simulations were performed using the CDOCKER protocol within Discovery Studio (Biovia Inc., USA).[36] The final retained poses were also manually inspected to confirm chemically reasonable geometries, preservation of key contacts in the hinge/DFG region, and absence of severe atom–atom clashes; the selected pose of **4c** was then used for the interaction analysis shown in Fig. 2 and 3.

Protein preparation. The X-ray crystal structure of the human RET kinase domain in complex with selpercatinib (PDB ID: 7JU6) was used as the template for wild-type docking. The protein was prepared by removing water molecules and the co-crystallized ligand, followed by the addition of hydrogen atoms and assignment of protonation states at pH 7.4. The structure was then subjected to a constrained energy minimization. The RET V804L mutant model was generated *via in silico* mutagenesis of the prepared 7JU6 structure, followed by local energy minimization of the residues surrounding the mutation site.

Ligand preparation. The 3D structures of all synthesized compounds were built and energy-minimized using the appropriate force field.

Docking protocol. The CDOCKER algorithm, a CHARMm-based molecular dynamics method,[36] was employed. The binding site was defined by a sphere centered on the co-crystallized ligand in the 7JU6 structure. For each ligand, 10 random starting conformations were generated and subjected to high-temperature molecular dynamics. Each conformation was then subjected to simulated annealing. The final poses were energy-minimized, and the top 10 poses for each ligand were saved and ranked based on their CDOCKER interaction energy. The resulting complexes were visually inspected to analyse key interactions.

4. Conclusions

In this study, we have successfully designed and synthesized a novel series of isoindigo-based derivatives as potent inhibitors of RET kinase. The biological evaluation identified compound **4c** as an early lead with promising biochemical potency, demonstrating low-nanomolar inhibition of both wild-type RET ($IC_{50} = 13.7$ nM) and retained, even enhanced, activity against the V804L gatekeeper mutant ($IC_{50} = 5.2$ nM). Furthermore, the series displayed a favorable selectivity profile, particularly with its negligible activity against c-KIT.

Molecular docking studies provided a clear structural rationale for the observed structure–activity relationships. The potent activity of **4c** is attributed to its ability to form key hydrogen bonds with the side chain of DFG Asp892, complemented by extensive hydrophobic interactions within the ATP-binding site. Importantly, the docking analysis revealed that the isoindigo scaffold can effectively adapt to the steric changes imposed by the V804L mutation, explaining its retained and even enhanced potency.

The dual activity of compound **4c** against both wild-type and the V804L gatekeeper mutant RET kinase supports the isoindigo scaffold as a promising starting point for this class of inhibitors. The activity of this series against TRKC and FLT3 D835Y also warrants further investigation. It is important to acknowledge that the current study is based entirely on biochemical (enzymatic) assays. No cell-based experiments, such as antiproliferative assays or phospho-RET inhibition in RET-driven cell lines, have been performed. Therefore, the translational relevance of these findings remains to be established. Future work will focus on evaluating compound **4c** in RET-driven cancer cell models (both wild-type and V804L-mutant), including antiproliferative and phospho-RET inhibition assays, synthesizing additional analogues around the *N*-methyl sulfonamide moiety to further optimize the lead, and profiling its activity against a broader panel of kinases to fully define its selectivity and therapeutic potential.

Conflicts of interest

The authors declare that there are no conflicts of interest.

Data availability

The datasets generated during and/or analysed during the current study are available from the corresponding author on reasonable request.

Supplementary information (SI): dose–response curves, molecular docking analysis, calculated enthalpic binding energies, and full spectroscopic characterization data (NMR

and mass spectrometry) for the synthesized compounds. See DOI: https://doi.org/10.1039/d6ra01152g.

Acknowledgements

This research project was fully funded by the Deanship of Scientific Research at Al-Ahliyya Amman University, Amman 19111, Jordan (Grant Number: 12/1130). The authors would like to thank Dr Areej Jaber for her technical help.

References

1 M. M. Al-Mahadeen, A. M. Jaber, R. A. Al-Qawasmeh and M. O. Taha, *J. Chem. Res.*, 2024, **48**, 17475198241262467.
2 M. Ahmad, B. Al-Najjar and A. Shakya, *Pharmacia*, 2024, **71**, 1–9.
3 Y. Hong, J. He, D. Deng, Q. Liu, X. Zu and Y. Shen, *J. Transl. Med.*, 2025, **23**, 439.
4 A. T. Regua, M. Najjar and H. W. Lo, *Front. Oncol.*, 2022, **12**, 932353.
5 V. Subbiah and G. J. Cote, *Cancer Discov.*, 2020, **10**, 498–505.
6 Y. Zhang, W. H. Zheng, S. H. Zhou, J. L. Gu, Q. Yu, Y. Z. Zhu, Y. J. Yan, Z. Zhu and J. B. Shang, *Cell Commun. Signal.*, 2024, **22**, 460.
7 S. Hamidi and M. I. Hu, *Ann. Endocrinol.*, 2024, **85**, 118–126.
8 G. J. Cote, C. Evers, M. I. Hu, E. G. Grubbs, M. D. Williams, T. Hai, D. Y. Duose, M. R. Houston, J. H. Bui, M. Mehrotra, S. G. Waguespack, N. L. Busaidy, M. E. Cabanillas, M. A. Habra, R. Luthra and S. I. Sherman, *J. Clin. Endocrinol. Metab.*, 2017, **102**, 3591–3599.
9 D. M. Vodopivec and M. I. Hu, *Ther. Adv. Med. Oncol.*, 2022, **14**, 17588359221101691.
10 R. J. Clifton-Bligh, *Endocr. Relat. Cancer*, 2025, **32**, e240224.
11 M. F. Chen, M. Repetto, C. Wilhelm and A. Drilon, *Drugs*, 2024, **84**, 1035–1053.
12 U. Khatri, N. Dayal, X. Hu, E. Larocque, N. Naganna, T. Shen, X. Liu, F. W. Holtsberg, M. J. Aman, H. O. Sintim and J. Wu, *Mol. Cancer Therapeut.*, 2023, **22**, 717–725.
13 J. Shen, L. Chen, Y. Song, S. Chen, W. Guo and Y. Li, *AAPS Open*, 2024, **10**, 6.
14 S. Fancelli, E. Caliman, F. Mazzoni, M. Brugia, F. Castiglione, L. Voltolini, S. Pillozzi and L. Antonuzzo, *Cancers*, 2021, **13**(4 (5)), 1091.
15 D. Saha, K. R. Ryan, N. R. Lakkaniga, B. Acharya, N. G. Garcia, E. L. Smith and B. Frett, *J. Med. Chem.*, 2021, **64**, 11747–11773.
16 L. Zhang, M. Moccia, D. C. Briggs, J. B. Bharate, N. R. Lakkaniga, P. Knowles, W. Yan, P. Tran, A. Kharbanda, X. Wang, Y. K. Leung, B. Frett, M. Santoro, N. Q. McDonald, F. Carlomagno and H. Y. Li, *J. Med. Chem.*, 2022, **65**, 1536–1551.
17 B. Frett, F. Carlomagno, M. L. Moccia, A. Brescia, G. Federico, V. De Falco, B. Admire, Z. Chen, W. Qi, M. Santoro and H. Y. Li, *Angew Chem. Int. Ed. Engl.*, 2015, **54**, 8717–8721.
18 Y. R. Murciano-Goroff, C. J. Falcon, S. T. Lin, C. Chacko, G. Grimaldi, D. Liu, C. Wilhelm, A. Iasonos and A. Drilon, *J. Thorac. Oncol.*, 2023, **18**, 620–627.
19 M. Sassatelli, F. Bouchikhi, B. Aboab, F. Anizon, D. Fabbro, M. Prudhomme and P. Moreau, *Anti Cancer Drugs*, 2007, **18**, 1069–1074.
20 J. Tegethoff, R. Bischoff, S. Saleh, B. Blagojevic, K. H. Merz and X. Cheng, *Molecules*, 2017, **22**(9), 1546.
21 P. Dhokne, A. P. Sakla and N. Shankaraiah, *Eur. J. Med. Chem.*, 2021, **216**, 113334.
22 A. M. Saleh, A. Aljada, M. M. El-Abadelah, M. O. Taha, S. S. Sabri, J. A. Zahra and M. A. Aziz, *Cell. Physiol. Biochem.*, 2015, **35**, 1943–1957.
23 M. A. Sulaibi, J. Zahra, S. Bardaweel, M. El Abadleh and M. O. Taha, *Med. Chem. Res.*, 2024, **33**, 1242–1266.
24 F. Bouchikhi, F. Anizon and P. Moreau, *Eur. J. Med. Chem.*, 2008, **43**, 755–762.
25 H. H. Li, X. H. Zheng, J. Z. Tan, L. L. Chen, H. Liu, X. M. Luo, X. Shen, L. P. Lin, K. X. Chen, J. Ding and H. L. Jiang, *Acta Pharmacol. Sin.*, 2007, **28**, 140–152.
26 H. Guan, A. D. Laird, R. A. Blake, C. Tang and C. Liang, *Bioorg. Med. Chem. Lett.*, 2004, **14**, 187–190.
27 X. Deng, W. Zhou, E. Weisberg, J. Wang, J. Zhang, T. Sasaki, E. Nelson, J. D. Griffin, P. A. Jänne and N. S. Gray, *Bioorg. Med. Chem. Lett.*, 2012, **22**, 4579–4584.
28 A. Gazit, K. Yee, A. Uecker, F. D. Böhmer, T. Sjöblom, A. Ostman, J. Waltenberger, G. Golomb, S. Banai, M. C. Heinrich and A. Levitzki, *Bioorg. Med. Chem.*, 2003, **11**, 2007–2018.
29 A. A. Warkentin, M. S. Lopez, E. A. Lasater, K. Lin, B. L. He, A. Y. Leung, C. C. Smith, N. P. Shah and K. M. Shokat, *Elife*, 2014, **3**(22), e03445.
30 S. Pathania, O. T. Pentikäinen and P. K. Singh, *Biochim. Biophys. Acta, Rev. Cancer*, 2021, **1876**, 188631.
31 A. Galanis and M. Levis, *Haematologica*, 2015, **100**, e77–e79.
32 G. H. Liu, T. Chen, X. Zhang, X. L. Ma and H. S. Shi, *MedComm*, 2022, **3**, e181.
33 A. E. Yesilkanal, G. L. Johnson, A. F. Ramos and M. R. Rosner, *J. Biol. Chem.*, 2021, **297**, 101128.
34 L. Sun, N. Tran, C. Liang, F. Tang, A. Rice, R. Schreck, K. Waltz, L. K. Shawver, G. McMahon and C. Tang, *J. Med. Chem.*, 1999, **42**, 5120–5130.
35 H. Ma, S. Deacon and K. Horiuchi, *Expet Opin. Drug Discov.*, 2008, **3**, 607–621.
36 G. Wu, D. H. Robertson, C. L. Brooks 3rd and M. Vieth, *J. Comput. Chem.*, 2003, **24**, 1549–1562.